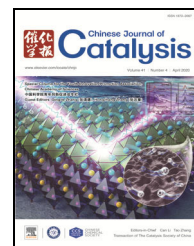


available at www.sciencedirect.comjournal homepage: www.elsevier.com/locate/chnjc

Article

Insight into catalytic properties of $\text{Co}_3\text{O}_4\text{-CeO}_2$ binary oxides for propane total oxidation

Wenjun Zhu ^{a,b}, Xiao Chen ^a, Jianhui Jin ^a, Xin Di ^a, Changhai Liang ^{a,*}, Zhongmin Liu ^{b,#}

^a State Key Laboratory of Fine Chemicals & Laboratory of Advanced Materials and Catalytic Engineering, Dalian University of Technology, Dalian 116024, Liaoning, China

^b Methanol to Olefins National Engineering Laboratory, Dalian National Laboratory for Clean Energy, Dalian Institute of Chemical Physics, Chinese Academy of Sciences, Dalian 116023, Liaoning, China

ARTICLE INFO

Article history:

Received 22 August 2019

Accepted 30 September 2019

Published 5 April 2020

Keywords:

Propane

Total oxidation

 $\text{Co}_3\text{O}_4\text{-CeO}_2$ *In-situ* DRIFTS

Volatile organic compounds

ABSTRACT

A series of $\text{Co}_3\text{O}_4\text{-CeO}_2$ binary oxides with various $\text{Co}/(\text{Ce}+\text{Co})$ molar ratios were synthesized using a citric acid method, and their catalytic properties toward the total oxidation of propane were examined. The activities of the catalysts decrease in the order $\text{CoCeO}_x\text{-70} > \text{CoCeO}_x\text{-90} > \text{Co}_3\text{O}_4 > \text{CoCeO}_x\text{-50} > \text{CoCeO}_x\text{-20} > \text{CeO}_2$. $\text{CoCeO}_x\text{-70}$ ($\text{Co}/(\text{Ce}+\text{Co}) = 70\%$ molar ratio) exhibits the highest catalytic activity toward the total oxidation of propane, of which the T_{90} is $310\text{ }^\circ\text{C}$ ($\text{GHSV} = 120000\text{ mL h}^{-1}\text{ g}^{-1}$), which is $25\text{ }^\circ\text{C}$ lower than that of pure Co_3O_4 . The enhancement of the catalytic performance of $\text{CoCeO}_x\text{-70}$ is attributed to the strong interaction between CeO_2 and Co_3O_4 , the improvement of the low-temperature reducibility, and the increase in the number of active oxygen species. *In-situ* DRIFTS and reaction kinetics measurement reveal that Ce addition does not change the reaction mechanism, but promotes the adsorption and activation of propane on the catalyst surface. The addition of water vapor and CO_2 in reactant gas has a negative effect on the propane conversion, and the catalyst is more sensitive to water vapor than to CO_2 . In addition, $\text{CoCeO}_x\text{-70}$ exhibits excellent stability and reusability in water vapor and CO_2 atmosphere.

© 2020, Dalian Institute of Chemical Physics, Chinese Academy of Sciences.

Published by Elsevier B.V. All rights reserved.

1. Introduction

Volatile organic compounds (VOCs), as the major contributors to global air pollution, have caused serious environmental problems in recent years. They are emitted from various sources, such as chemical plants, power stations, oil refineries, and vehicle exhausts [1]. Over time, environmental legislation on the permissible levels of atmospheric emission has become increasingly stringent; consequently, the usage of liquefied petroleum gas (LPG) and liquefied natural gas (LNG) as alternatives in gasoline and diesel vehicles is increasing. Moreover,

the amount of light alkanes released from stationary sources is increasing with the rapid development of chemical technology [2]. Due to the stability of the molecular structure of light alkanes, their elimination is considerably difficult. Therefore, developing a highly efficient purification technology for the control of light alkane emissions is urgent and necessary.

Nowadays, adsorption, membrane separation, photo-catalysis, catalytic oxidation, and plasma oxidation are being used to control the emissions of light alkanes [3]. Catalytic oxidation, as a significant technique for converting pollutants totally into water and carbon dioxide, is considered one of the

* Corresponding author. Fax: +86-411-84986353; E-mail: changhai@dlut.edu.cn# Corresponding author. Fax: +86-411-84379998; E-mail: liuzm@dicp.ac.cn

This work was supported by the National Key R&D Program of China (2016YFB0600305).

DOI: S1872-2067(19)63523-0 | <http://www.sciencedirect.com/science/journal/18722067> | Chin. J. Catal., Vol. 41, No. 4, April 2020

most efficient routes for light alkane elimination due to its low reaction temperature, low operating cost, and zero auxiliary fuels [4,5]. Owing to the dependence of catalytic oxidation on catalysts, the search for high activity, better stability, and low-cost catalysts is attracting much attention. Although noble metal catalysts, such as Pd and Pt, are supposed to be highly active and stable, their high expense, sintering rates, volatility, and the possibility of being poisoned by water or sulfur compounds limit their wide practical application [6–8]. In recent years, intensive efforts have been devoted to the synthesis of transition and rare earth metal oxides as alternatives to noble metal catalysts and for the reduction of the reaction temperature [9–11].

Cobalt oxide (CoO_x) and cerium oxide (CeO_x) are the common choices for the catalytic oxidation of VOC. Co₃O₄ is known as an active and prevalent catalyst for CO and VOC catalytic oxidation at low temperatures [12–14]. Different polymorphs of Co₃O₄ and Co₃O₄-MO_x binary oxides have been reported as effective and stable catalysts for the total oxidation of propane [15,16]. Zheng et al. [15] reported that doping Ni into spinel Co₃O₄ lattice resulted in 100% propane conversion at the temperature below 400 °C, and the reaction kinetics were also enhanced owing to the improvement of the surface lattice oxygen activity. CeO₂, known as a rare earth oxide, has been widely used as a significant component or structural and electronic promoter of heterogeneous catalysts owing to its excellent oxygen storage capacity (OSC) [17–19]. Molecular oxygen can easily be diverted to the CeO₂ surface through the rapid and reversible redox of Ce⁴⁺ and Ce³⁺ [20]. Recently, catalytic synergistic effects between Co and Ce oxides have been found in various reactions, such as methane combustion [17], N₂O decomposition [21], and formaldehyde oxidation [22]. Therefore, Co₃O₄-CeO₂ binary oxides may be potential catalysts for the catalytic oxidation of light alkanes.

Propane, a typical kind of light alkane, is common in automobile exhaust systems (LPG automobile) and the exhaust gas of some chemical factories (production of epoxy propane/styrene, phenol acetone, and acrylic acid). The molecular structure of propane is very stable, which can well represent the characteristic of light alkanes. Therefore, Co₃O₄-CeO₂ binary oxide catalysts were synthesized by the citric acid method and applied to propane catalytic oxidation to study the correlation among the composition, structure, and the catalytic performances of the catalysts. The reaction kinetics and reaction mechanism for the total oxidation of propane over Co₃O₄-CeO₂ catalysts are further studied. In addition, the effects of CO₂ and water vapor on the propane conversion and stability of the catalyst have been investigated.

2. Experimental

2.1. Catalyst preparation

Co₃O₄-CeO₂ binary oxides with various Co/(Ce+Co) molar ratios from 0 to 100% (labeled as CoCeO_x-0 and CoCeO_x-100) were synthesized by the citric acid method. Typically, for the CoCeO_x-70 sample, 3 mmol of Ce(NO₃)₃·6H₂O and 7 mmol of

Co(NO₃)₃·6H₂O were dissolved in 20 mL of deionized water. An excess amount of citric acid solution (citric acid/metal = 1.5, molar ratio) was added to the above solution. Thereafter, the mixture was stirred at 60 °C for 1 h and rotary-evaporated to produce a gel-like substance. The substance was dried at 90 °C overnight and transferred to a muffle furnace at 300 °C for 1 h to decompose citric acid. Finally, the powder was ground and calcined at 550 °C for 4 h.

2.2. Characterization methods

X-ray diffraction (XRD) patterns were recorded using a Smart-Lab 9KW diffractometer with Cu Kα₁ radiation (λ = 1.54178 Å). N₂ physisorption measurements were conducted on a Quantachrome Autosorb-iQ instrument, and the specific surface area was obtained according to the Brunauer-Emmett-Teller (BET) method. Raman spectra were acquired using a laser confocal micro-Raman instrument (Thermo Fisher Scientific). XPS measurement was performed on an ESCALAB250 instrument (Thermo-VG Scientific). The morphologies and microstructure of the sample were characterized by scanning electron microscopy (SEM, FEI QUANTA 450) and transmission electron microscopy (TEM, FEI TECNAI 20S-TWIN), respectively. H₂-TPR and O₂-TPD experiments were carried out on an automatic chemical adsorption instrument (Quantachrome OBP-1). C₃H₈-TPSR experiment was carried out in a quartz reactor connected to a mass spectrometer (GSD 320 OMNISTAR). *In-situ* DRIFTS analysis was conducted on an FTIR spectrometer (Thermo fisher Nicolet iS50) equipped with an MCT/A detector in the 650–4000 cm⁻¹ range. Detailed characterization methods are described in Supporting Information.

2.3. Catalytic performance evaluation

The catalytic activity of the Co₃O₄-CeO₂ binary oxide catalysts toward the total oxidation of propane was evaluated in a fixed-bed reactor. The catalyst sample (0.1 g) was placed in the reactor (10 mm i.d.) for each reaction. The reactant gas consisted of 0.2 vol.% C₃H₈, 5 vol.% O₂, and balanced with Ar at a total flow rate of 200 mL min⁻¹ (GHSV = 120000 mL h⁻¹ g⁻¹). Catalytic performance was evaluated with the programmed temperature from 100 to 500 °C (2 °C min⁻¹). The concentration of C₃H₈ in the reactant gas was detected using an online gas chromatograph (GC-7900) with an FID detector. The C₃H₈ conversion (X%) was determined using Equation (1), as follows:

$$X\% = \frac{C_3H_8^{in} - C_3H_8^{out}}{C_3H_8^{in}} \times 100\%, \quad (1)$$

where C₃H₈ⁱⁿ and C₃H₈^{out} are the concentrations of C₃H₈ in the inlet and outlet gas, respectively, and T₁₀, T₅₀, and T₉₀ represent the reaction temperature for 10%, 50%, and 90% C₃H₈ conversions, respectively.

2.4. Reaction kinetics

The reaction order for each catalyst was measured in the above fixed-bed reactor at normal pressure. The reactant gas

was composed of x vol.% C_3H_8 and y vol.% O_2 , balanced with Ar (200 mL min^{-1}). For each test, 0.05 g of the catalyst was diluted with 1 mL of quartz sand (60–80 mesh), and propane conversion was restricted below 15%. The reaction order of every catalyst was obtained using the following formula:

$$r = k(P_{C_3H_8})^\alpha(P_{O_2})^\beta \quad (2)$$

where $P_{C_3H_8}$ and P_{O_2} represent the partial pressures of C_3H_8 and O_2 in the reactant gas, respectively. The values α and β are the partial reaction orders of C_3H_8 and O_2 , respectively. The α values were determined by varying the concentration of C_3H_8 (x vol.%) to achieve the partial pressure of C_3H_8 between 0.1 and 0.8 kPa when the flow rate (200 mL min^{-1}) and oxygen partial pressure (5.0 kPa) remained unchanged. Similarly, the β values were obtained by varying the concentration of O_2 (y vol.%) to achieve the oxygen partial pressure between 2.0 to 8.0 kPa at a fixed C_3H_8 pressure (0.2 kPa).

3. Results and discussion

3.1. Characterizations of Co_3O_4 - CeO_2 binary oxides

The XRD patterns of CeO_2 , Co_3O_4 , and Co_3O_4 - CeO_2 binary oxides are illustrated in Fig. 1a. Two diffraction peaks corresponding to CeO_2 and Co_3O_4 are found for all the Co_3O_4 - CeO_2 binary oxides. All the diffraction peaks of Co_3O_4 and CeO_2 can be ascribed to the Co_3O_4 spinel structure (JCPDS 43–1003) and CeO_2 cubic fluorite structure (JCPDS 34–0349), respectively. The crystallite sizes and the specific surface area of all samples are listed in Table 1. It can be found that the Co_3O_4 - CeO_2 binary oxides exhibit smaller crystallite sizes of CeO_2 (8.7 nm) and Co_3O_4 (11.4 nm) than those of single CeO_2 (18.8 nm) and Co_3O_4 (31.0 nm), and their specific surface areas increase with respect to those of single CeO_2 ($39 \text{ m}^2 \text{ g}^{-1}$) and Co_3O_4 ($13 \text{ m}^2 \text{ g}^{-1}$). These results demonstrate that the interaction of Ce and Co could restrain the growth of the crystallite and increase the specific surface area. In addition, the crystallite size of CeO_2 (8.7 nm) is nearest to that of Co_3O_4 (11.4 nm) when the Co/(Ce+Co) molar ratio is 70%. This suggests the better dispersion of CeO_2 and Co_3O_4 crystallites over that of the $CoCeO_x$ -70 catalyst, which contributes to improving the interaction between CeO_2 and Co_3O_4 [17].

Fig. 1b shows the Raman spectra of the Co_3O_4 - CeO_2 binary oxides. The band at ca. 462 cm^{-1} detected in pure CeO_2 is as-

cribed to the F_{2g} symmetric O–Ce–O stretching vibration of CeO_2 with a cubic fluorite symmetric structure [23]. For the Co_3O_4 sample, there are five peaks at 194, 482, 522, 619, and 694 cm^{-1} , corresponding to the F_{2g}^1 , E_g , F_{2g}^2 , F_{2g}^3 , and A_{1g} modes of the Co_3O_4 with spinel structure, respectively [24,25]. The effects of the cations and isomorphous isotope replacement show that the 694 cm^{-1} vibration is characteristic of the sub-lattice (octahedral/tetrahedral), where the highest-valence cations are located [25]. With the increase in the Ce content from Co_3O_4 to $CoCeO_x$ -20, the A_{1g} vibration (694 cm^{-1}) slightly shifts toward lower wavenumbers, and the peak becomes asymmetric and smaller. Since the slight differences in the vibration are connected to the residual stress or lattice distortion of the structure, the intensity of the Raman spectra depends on the grain size and morphology [26]. The changes of the A_{1g} vibration may be ascribed to the distortion of the Co_3O_4 lattice and aggregation of CeO_2 on the surface. This effect could result in increased concentration of Co at low oxidation state and, in turn, indicate an increased amount of oxygen defects. Moreover, the bands corresponding to CeO_2 also slightly shift toward lower wavenumbers when the Co content is 20%, indicating that some amount of Co can be incorporated into the CeO_2 lattice and deform the crystal lattice. All these results indicate that lattice distortion or residual stress exists in the Co_3O_4 - CeO_2 binary oxides, which can activate gas oxygen and offer lattice sites for oxygen migration.

To investigate the morphology of the samples, the TEM images of Co_3O_4 , CeO_2 , and $CoCeO_x$ -70 catalysts are shown in Fig. 2. The particle sizes of Co_3O_4 (Fig. 2a) and CeO_2 (Fig. 2c) are ca. 40 nm and ca. 18 nm, respectively. For the $CoCeO_x$ -70 sample, the particle size significantly decreases and, the boundary between the nanoparticles becomes obscure with uniform size distribution. The HRTEM characterization of $CoCeO_x$ -70 (Fig. 2e) clearly shows several lattice fringes of the crystallinity of oxides, with the d-spacing of 0.24 nm indexed to the (311) crystal plane of spinel Co_3O_4 , and the d-spacing of 0.31 nm indexed to the (111) crystal plane of cubic CeO_2 . These results indicate that cubic fluorite CeO_2 and spinel Co_3O_4 coexist in the $CoCeO_x$ -70 catalyst, agreeing with the XRD analysis. Moreover, Fig. 2e clearly shows that there is an interface between Co_3O_4 nanoparticles and CeO_2 nanoparticles in binary oxides. The elemental mapping image and EDX line-scan analysis (Fig. S1) confirm the uniform distribution of Co, Ce, and O elements over

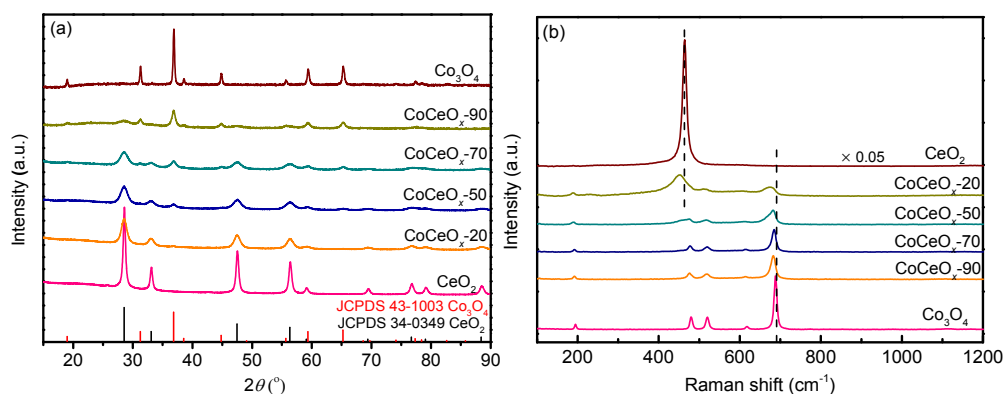


Fig. 1. XRD patterns (a) and Raman spectra (b) of Co_3O_4 - CeO_2 binary oxides.

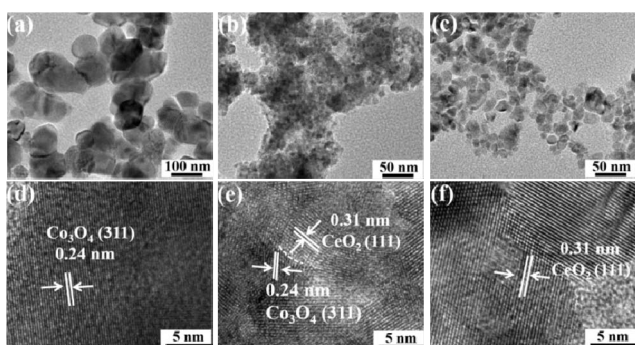


Fig. 2. TEM and HRTEM images of (a, d) Co_3O_4 , (b, e) CoCeO_x -70, (c, f) CeO_2 .

CoCeO_x -70, and the $\text{Co}/(\text{Ce}+\text{Co})$ molar ratio (ca. 67%) is close to the theoretical value (70%). The SEM and EDX experiments (Fig. S2) show that the CoCeO_x -70 catalyst features an irregular shape with a uniform distribution of elements on its surface. Consequently, it can be concluded that the CoCeO_x -70 binary oxide shows a uniform element distribution in nanometer and micrometer sizes, which may be attributed to the role of citric acid as a chelating agent and for minimizing the phase separation of the components.

The H_2 -TPR profiles of CeO_2 , Co_3O_4 , and Co_3O_4 - CeO_2 binary oxides are shown in Fig. 3. Two reduction peaks were observed for the signal CeO_2 reduction process, the first peak at ca. 550 °C is assigned to the reduction of the surface oxygen species (lattice oxygen), while the second peak above 800 °C is attributed to the reduction of bulk oxygen [17]. However, there is only one broad peak (300–550 °C) for the reduction of single Co_3O_4 and no traces of chemisorbed oxygen reduction. It is reported that large particles of Co_3O_4 are often directly reduced to metal Co through a one-step process [10,21,27]. In our research, the broad peak has been split into three peaks. Considering the total reduction of Co_3O_4 and stoichiometry of the reduction, peak I corresponds to the reduction of Co^{3+} to Co^{2+} , and the process of $\text{Co}^{3+}/\text{Co}^{2+}$ to Co is the sum of peak II. With the incorporation of Ce into Co_3O_4 , multiple reduction peaks generate and the peak position changes accordingly. The reason is

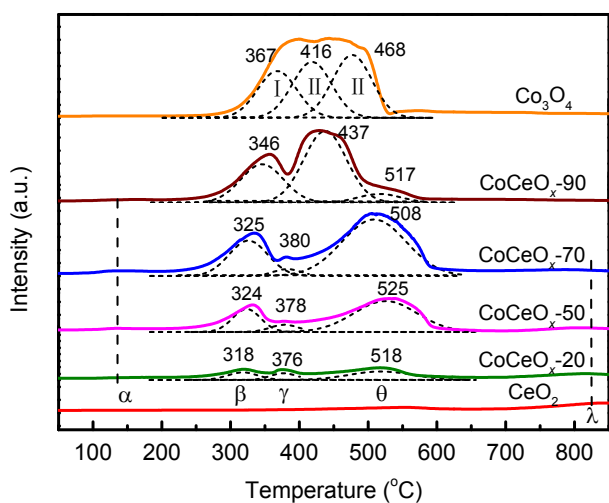


Fig. 3. H_2 -TPR profiles of CeO_2 , Co_3O_4 , and Co_3O_4 - CeO_2 binary oxides.

that the fine particles of Co_3O_4 interacting with CeO_2 appear to be reduced in a two-step process. The first is promoted by the interaction between CeO_2 and Co_3O_4 , which is probably attributed to the binding energy of the Co-O bond. The second is hindered by the stabilizing action of CeO_2 to Co ions with intermediate valency [27,28]. Moreover, the reduction peaks above 800 °C for all the Co_3O_4 - CeO_2 binary oxides are attributed to the bulk oxygen reduction of CeO_2 , and the peaks below the temperature are primarily connected with the Co_3O_4 phase, which has greater reducibility than CeO_2 . Meanwhile, the reduction peaks of Co_3O_4 could overlap the peaks of CeO_2 since the reduction of CeO_2 consumes less H_2 than that in the case of Co_3O_4 . Based on the above, the reduction peaks for the Co_3O_4 - CeO_2 binary oxides with respect to the temperature are assigned in the following: peak α (below 200 °C) – surface adsorbed oxygen species; peak β (250–350 °C) – Co^{3+} at the interface between Co_3O_4 and CeO_2 reduction to Co^{2+} ; peak γ (360–450 °C) – independent Co_3O_4 weakly interacting with CeO_2 reduction to metallic Co; peak θ (450–600 °C) – Co^{2+} interacting with CeO_2 reduction to Co; peak λ (above 800 °C) – the bulk oxygen reduction of CeO_2 .

Notably, among all the Co_3O_4 - CeO_2 binary oxides, the intensity of peak α for CoCeO_x -70 is the highest, which indicates that CoCeO_x -70 has the most adsorbed oxygen species. Moreover, the β reduction peaks slightly shift toward lower temperatures and their intensities simultaneously decrease with the increase in the Ce content (As shown in Table 1). The downshift and reduction of the β peaks are related to the amount of Co^{3+} at the interface between CeO_2 and Co_3O_4 . Considering the amount of Co_3O_4 in the Co_3O_4 - CeO_2 binary oxides, the highest relative intensity of peak β (1.3) is found on the CoCeO_x -70 catalyst. In other words, CoCeO_x -70 has the highest proportion of Co^{3+} with respect to Co_3O_4 among all the catalysts, which is probably due to the strong interaction between Co_3O_4 and CeO_2 . Since peak α and peak β correlate with the catalytic activity [13], it is reasonable to infer that the Co_3O_4 - CeO_2 binary oxides, particularly the CoCeO_x -70 catalyst, may contain more easily redox species, and may thus improve the catalytic activity toward the catalytic oxidation of propane.

The C_3H_8 -TPSR experiment is carried out to further detect the redox properties of Co_3O_4 - CeO_2 . The MS signals of H_2O ($m/z = 18$), C_3H_8 ($m/z = 43$), and CO_2 ($m/z = 44$) are shown in Fig. 4. The results show that no reaction product is detected for pure CeO_2 within the testing temperature range of 100–500 °C, indicating that CeO_2 is almost inactive at temperatures below 500 °C. For the Co_3O_4 catalyst, two positive broad peaks at 433 and 452 °C in the curves of CO_2 and H_2O are observed, and a negative peak at 435 °C in the C_3H_8 curve is also found, suggesting that the total oxidation of propane occurs on the Co_3O_4 surface at this temperature. Similar results are found in the Co_3O_4 - CeO_2 binary oxides; however, the peak at < 450 °C shifts toward lower temperature and a narrow peak appears at > 450 °C. The broad peaks below 450 °C are attributed to the reaction of propane with the lattice oxygen species in Co_3O_4 interacting with CeO_2 . Conversely, the narrow peaks above 450 °C are due to the consumption of the lattice oxygen in CoO stabilized by CeO_2 [12]. The downward shift of the peaks (< 450 °C) upon

Table 1
Textural properties, XPS, and H₂-TPR results of CeO₂, Co₃O₄, and Co₃O₄-CeO₂ binary oxides.

Catalyst	A _{BET} / (m ² g ⁻¹)	D _a ^a (nm)	D _b ^a (nm)	XPS resolving			H ₂ -TPR				
				O _{ads} (eV)	O _{latt} (eV)	O _{ads} /O _{latt}	Co ³⁺ /Co ²⁺	Ce ³⁺ /(Ce ⁴⁺ +Ce ³⁺)	β(I) (°C)	A (β) ^b	R (β) ^c
Co ₃ O ₄	13	—	31.0	531.4	529.9	0.31	0.88	—	367	1	1
CoCeO _x -90	40	8.7	14.4	531.4	529.7	0.32	1.01	19.6	346	0.81	1.1
CoCeO _x -70	39	8.7	11.4	531.4	529.7	1.08	1.15	20.8	325	0.68	1.3
CoCeO _x -50	43	8.9	12.4	531.4	529.4	0.29	0.86	19.3	324	0.36	1.1
CoCeO _x -20	50	10.0	13.9	531.2	529.1	0.28	—	18.6	318	0.11	1.1
CeO ₂	39	18.8	—	531.6	529.5	0.20	—	18.3	—	—	—

^a Crystallite sizes calculated from the line broadening of the (111) plane of CeO₂ and (311) plane of Co₃O₄, respectively.

^b Area of peak β; peak I area is a reference value of 1.

^c Relative area of peak β; the area of peaks β per unit Co₃O₄ mass: $R(\beta) = A_{\beta}/(A_{I} \cdot M_c\%)$, where $M_c\%$ is the mass fraction of Co₃O₄ in the Co₃O₄-CeO₂ binary oxides.

increasing the Ce content is mainly ascribed to the interaction between Co₃O₄ and CeO₂ that promotes the activation of oxygen species, while the decline in the peak intensity is due to the decrease in the Co₃O₄ amount in the binary oxides. Interestingly, the lowest temperature of the narrow peak is found on the CoCeO_x-70 sample, which indicates that its oxygen species are highly active to react with propane. In general, all the positive peaks of CO₂ are ascribed to the lattice oxygen species consumption, which is consistent with the Mars-van Krevelen mechanism that lattice oxygen species play an important role in catalytic oxidation of propane [29].

The O₂-TPD analysis is used to identify oxygen species and study the oxygen desorption behavior of the catalyst. In general, the adsorbed oxygen species are arranged as follows: O₂ (ad) → O₂⁻ (ad) → O⁻ (ad) → O²⁻ (lattice) [6,30]. As shown in Fig. 5, the peaks below 300 °C correspond to the desorption of the surface oxygen species (O₂⁻, O⁻), and the desorption peaks above 350 °C are attributed to the desorption of lattice oxygen [13]. For the Co₃O₄-CeO₂ binary oxides, it is found that peak β shifts toward lower temperatures, and peak α splits into two peaks (α₁ and α₂). These changes can be ascribed to the interaction between Co₃O₄ and CeO₂. Considering the thermostability of the adsorbed oxygen species, peaks α₁ and α₂ are assigned to the desorption of adsorbed O₂⁻ and O⁻ species, respectively. For peak α (O₂⁻ and O⁻), a relatively low-beginning temperature and high peak intensity are found for the CoCe-

O_x-70 catalyst. Large intensities of the desorption peaks and low beginning oxygen desorption temperatures could result in improved catalytic oxidation activity [31]. It can be concluded that CoCeO_x-70 has abundant active oxygen species on its surface and may have better catalytic performance toward the total oxidation of propane.

The XPS spectra of O 1s, Co 2p, and Ce 3d for CeO₂, Co₃O₄, and Co₃O₄-CeO₂ binary oxides are shown in Fig. 6. The single lobed asymmetric peak of the O 1s spectra (Fig. 6a) confirms the existence of several kinds of surface oxygen species with different chemical states [32]. The O 1s spectra is split into three peaks: the peak at ~529.7 eV is attributed to the lattice oxygen (O_{latt}), the peak at ~531.4 eV corresponds to the surface adsorbed oxygen (O_{ads}), and the peak at ~532.7 eV is connected to the adsorbed OH groups or carbonate species [33,34]. The surface O_{ads}/O_{latt} molar ratio of CoCeO_x-70 (1.08) is much higher than those of other samples, indicating that the CoCeO_x-70 catalyst has a relatively high amount of electrophilic oxygen species on its surface, which is beneficial for deep oxidation reactions. The results are consistent with the O₂-TPD analysis results that CoCeO_x-70 has a high number of oxygen species at relatively low temperatures. In addition, the O 1s peak shift is associated with the charge of oxide ions, which may be affected by the surrounding chemical environment. Therefore, the shift of the O 1s peak here should be attributed to the interaction

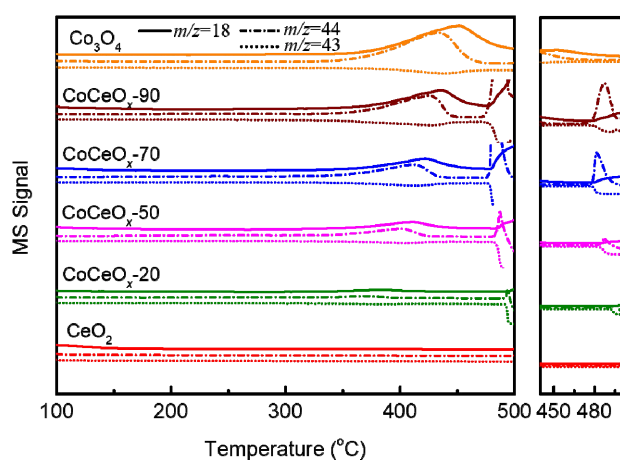


Fig. 4. C₃H₈-TPSR experiments over the CeO₂, Co₃O₄, and Co₃O₄-CeO₂ binary oxides.

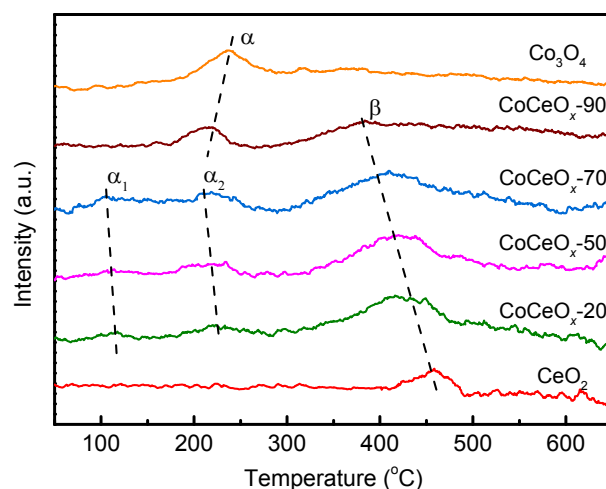


Fig. 5. O₂-TPD profiles of CeO₂, Co₃O₄, and Co₃O₄-CeO₂ binary oxides.

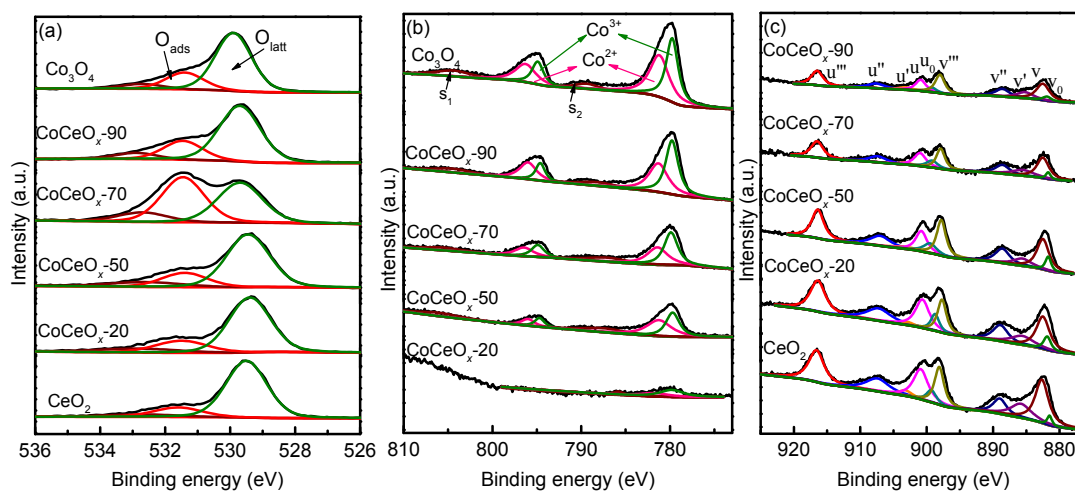


Fig. 6. XPS spectra of O 1s (a), Co 2p (b), and Ce 3d (c) for CeO₂, Co₃O₄, and Co₃O₄-CeO₂ binary oxides.

between CeO₂ and Co₃O₄.

Fig. 6b illustrates the Co 2p spectra of all the samples. All the Co 2p spectra show two broad and asymmetric peaks, which are separated by a spin-orbit splitting of ca. 15.1 eV and accompanied by two shake-up satellites (S₁, S₂). The Co 2p_{3/2} signal at BE = 779.7 eV demonstrates the existence of Co³⁺ on the surface, while the Co 2p_{1/2} signal at BE = 781.5 eV indicates the existence of Co²⁺ on the surface [35]. By curve-fitting the Co 2p peaks (Table 1), the Co³⁺/Co²⁺ ratio increases from 0.86 to 1.15, and subsequently decreases to 0.88 with increasing Co/(Ce+Co) ratios. It is reported that Co³⁺ is active for CO oxidation, whereas Co²⁺ is almost inactive [12]. The Co ions in the CoCeO_x-70 catalyst has abundant Co³⁺ sites (Co³⁺/Co²⁺ = 1.15), which will be beneficial for the catalytic oxidation of propane.

The Ce 3d_{5/2} and 3d_{3/2} XPS spectra are illustrated in Fig. 6c. The Ce 3d spectra can be resolved into ten peaks, where six peaks, denoted as v, v', v'', u, u'', and u''', are assigned to Ce⁴⁺, while the other four peaks, denoted as v₀, v', u₀, and u', are ascribed to Ce³⁺ [6]. The amount of surface Ce³⁺ ions is obtained according to the following formula:

$$C_{Ce^{3+}} = \frac{Ce^{3+}}{Ce^{3+} + Ce^{4+}} \quad (3)$$

where Ce³⁺ is the area sum of v₀, v', u₀, and u', and Ce⁴⁺ is the area sum of v, v', v'', u, u'', and u'''. The Ce³⁺ concentration is

related to the oxygen vacancies on the CeO₂ surface. As shown in Table 1, with the increase of the Co/(Ce+Co) ratio, the Ce³⁺ concentration increases from 18.3% to 20.8%, and thereafter drops to 19.6%. The highest C_{Ce³⁺} value (20.8%) is obtained on the CoCeO_x-70 surface, suggesting that the CoCeO_x-70 surface has the highest number of oxygen vacancies.

3.2. Catalytic activity and reaction kinetic study

The catalytic activities of the Co₃O₄-CeO₂ binary oxide catalysts toward the oxidation of propane are evaluated. As shown in Fig. 7a, single CeO₂ species exhibit low activity toward the total oxidation of propane, while single Co₃O₄ species occur with superior activity. The T₁₀, T₅₀, and T₉₀ values of the Co₃O₄-CeO₂ binary oxide catalysts are summarized in Table 2. Evidently, the presence of Co significantly enhances the catalytic activity, and the catalytic activity of the Co₃O₄-CeO₂ binary oxide catalysts exhibits a volcanic distribution: CoCeO_x-70 > CoCeO_x-90 > Co₃O₄ > CoCeO_x-50 > CoCeO_x-20 > CeO₂. Among the Co₃O₄-CeO₂ catalysts, CoCeO_x-70 exhibits the highest catalytic activity and its T₉₀ value is 310 °C, which is approximately 25 °C and 165 °C lower than those of the single Co₃O₄ and CeO₂ catalysts, respectively. In addition, the single Co₃O₄ and CeO₂ catalysts are mechanically mixed with the same molar ratios of

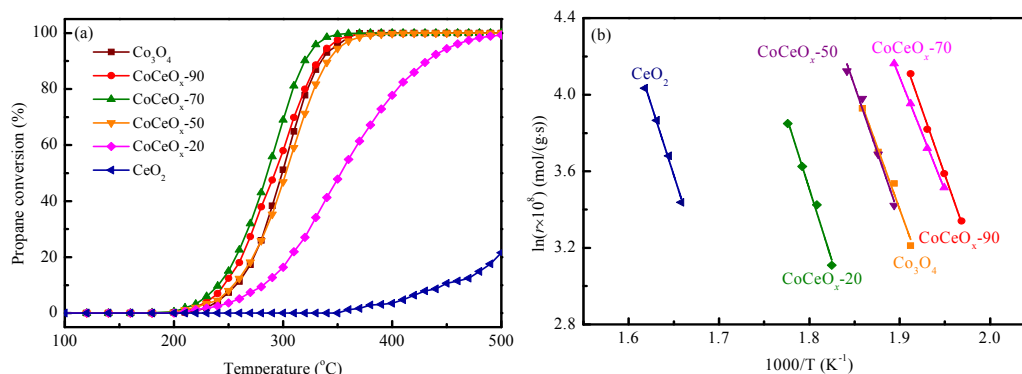


Fig. 7. (a) Activities of the Co₃O₄-CeO₂ binary oxide catalysts for the catalytic oxidation of propane; (b) Arrhenius plots for the catalytic oxidation of propane over Co₃O₄-CeO₂ binary oxide catalysts.

Table 2Catalytic performances of CeO₂, Co₃O₄, and Co₃O₄–CeO₂ binary oxide catalysts.

Catalyst	T_{10} (°C)	T_{50} (°C)	T_{90} (°C)	Reaction rate ^a ($r \times 10^7 \text{ mol g}^{-1} \text{ s}^{-1}$)	E_a (kJ mol ⁻¹)
CeO ₂	350	415	475	0	123
CoCeO _x -20	285	355	435	1.08	124
CoCeO _x -50	255	305	345	2.40	114
CoCeO _x -70	245	265	310	4.48	97
CoCeO _x -90	245	295	330	3.71	112
Co ₃ O ₄	255	300	335	2.11	108
CoCeO _x -70(M)	270	305	360	1.11	—

^aThe feed gas was 0.2% O₂ + 5% O₂/Ar, and $T = 250 \text{ }^\circ\text{C}$, GHSV = 120000 mL h g⁻¹.

CoCeO_x-70 and their catalytic activities toward the oxidation of propane are tested (shown in Fig. S3). CoCeO_x-70 shows a superior activity toward the total oxidation of propane to that of the mechanically mixed oxide CoCeO_x-70 (M), and its reaction rate at 250 °C is $4.48 \times 10^{-7} \text{ mol g}^{-1} \text{ s}^{-1}$, almost four times that of CoCeO_x-70 (M) ($1.11 \times 10^{-7} \text{ mol g}^{-1} \text{ s}^{-1}$). It can be deduced that the Co₃O₄–CeO₂ binary oxide catalysts synthesized by the citric acid method are not the simple mechanical mixing catalysts, and a strong surface mutual interaction exists between Co₃O₄ and CeO₂, which may improve the redox properties of the Co₃O₄–CeO₂ catalysts and subsequently enhance their catalytic activities. To study the intrinsic catalytic activities of the Co₃O₄–CeO₂ binary oxide catalysts toward the total oxidation of propane, the reaction rate and apparent activation energies (E_a) were evaluated, and the results are shown in Table 2 and Fig. 7b. It is observed that the reaction rate of CoCeO_x-70 ($4.48 \times 10^{-7} \text{ mol g}^{-1} \text{ s}^{-1}$) is the highest, and its corresponding E_a (97 kJ/mol) is the lowest among all the Co₃O₄–CeO₂ catalysts. These findings confirm that CoCeO_x-70 exhibits the highest catalytic activity and Ce promotes the intrinsic activity of the Co₃O₄ catalyst.

The reaction orders with respect to reactants C₃H₈ and O₂ are determined on the Co₃O₄ and CoCeO_x-70 catalysts (Figs. 8a and 8b). The reaction order of the propane catalytic oxidation on CoCeO_x-70 is calculated to be 0.37 with respect to C₃H₈, which is lower than that of the single Co₃O₄ catalyst (0.46). The result suggests that the adsorption and activation of propane

on CoCeO_x-70 catalyst are stronger than those on Co₃O₄ [9]. In addition, the reaction order of O₂ on CoCeO_x-70 (0.35) approximates to that of Co₃O₄ (0.34), suggesting that the incorporation of Ce is less sensitive to O₂ concentration. Moreover, the reaction orders of C₃H₈ and O₂ often display considerable differences in the literature date, even for the same catalytic system, which is due to the different experimental conditions [36]. Moro-oka et al. testified that the reaction orders of C₃H₈ and O₂ over Co₃O₄ catalysts strongly depend on the partial pressure, reaction temperature, and catalyst preparation method [37]. The zero-order dependence of the O₂ concentration suggests that lattice oxygen is the active oxygen species [25]. However, the order of O₂ is greater than zero in this study. It can be assumed that weakly bound oxygen species would participate in the reaction and serve as active species in the catalytic oxidation of propane.

3.3. Effects of CO₂ and water vapor concentrations and stability

Considering the inevitable existence of CO₂ and water vapor under practical conditions, variable concentrations of CO₂ and water vapor are added into the feed gas, respectively (Figs. 9a and 8b). The addition of water vapor and CO₂ in reactant gas has a negative effect on the propane conversion over CoCeO_x-70 catalyst, although its influence weakens with the increase in water vapor and CO₂ concentrations within the tested range. The negative effect could be attributed to the competitive adsorption of water vapor or CO₂, which decreases the number of active sites available for propane and O₂ [38,39]. Chemical equilibrium simultaneously accounts for the decline of propane conversion. Remarkably, the addition of water vapor has a more significant effect than that of CO₂ on the decline of propane conversion. As shown in Fig. S4, under the same concentration, the T_{50} and T_{90} values of CoCeO_x-70 in a water vapor condition are higher than those in a CO₂ condition. For example, the T_{50} and T_{90} values in water vapor condition (5 vol.%) are 310 °C and 350 °C, while those in CO₂ condition are 282 °C and 315 °C, respectively. This is probably due to the relatively strong adsorption of H₂O on the catalyst surface. In general, CoCeO_x-70 can maintain a high activity in CO₂ and water vapor atmosphere, and water vapor has a greater effect on the catalyst activity than CO₂.

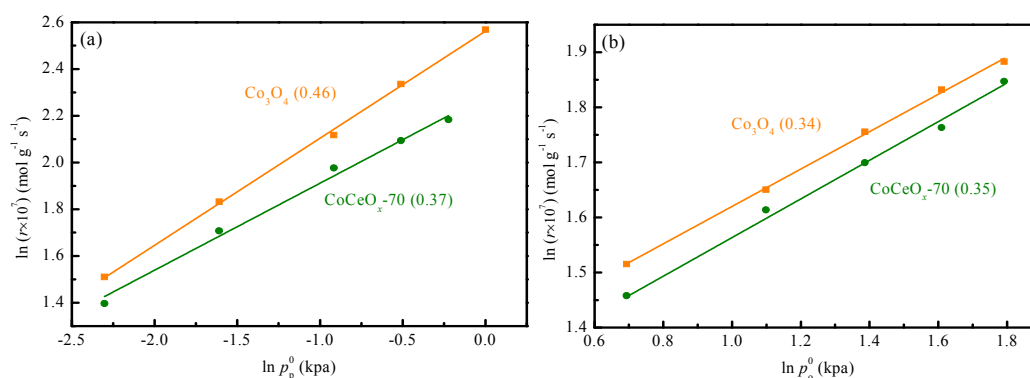


Fig. 8. Determination of the reaction order of C₃H₈ (a), O₂ (b) over the Co₃O₄ and CoCeO_x-70 catalysts.

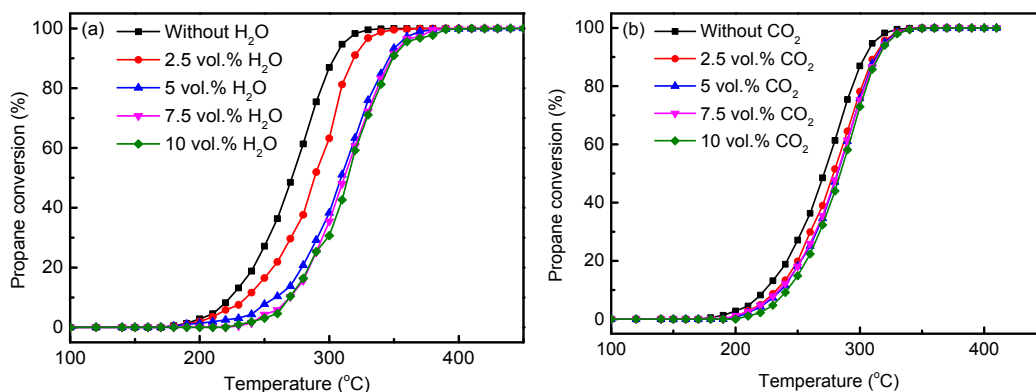


Fig. 9. Effects of water vapor concentration (a) and CO₂ concentration (b) on the catalytic activity over CoCeO_x-70.

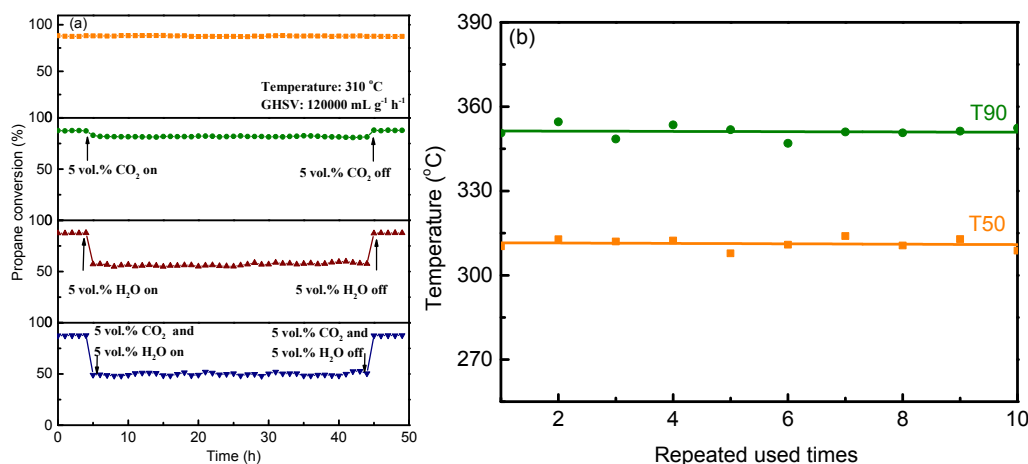


Fig. 10. (a) Stability of the CoCeO_x-70 catalyst in water vapor and CO₂ atmosphere; (b) Reusability of the CoCeO_x-70 catalyst under a humid condition (5 vol.% H₂O).

The stability of the CoCeO_x-70 catalyst is determined under severe conditions. As shown in Fig. 10a, the catalytic activity of the CoCeO_x-70 catalyst hardly changes after 50 h at 310 °C. When 5 vol.% CO₂ is added into the reactant gas, the propane conversion drops slightly (ca. 5%) but remains constant for 40 h, and recovers back to the original value in the absence of 5 vol.% CO₂. A similar result is achieved when 5 vol.% water vapor is added into the reactant gas during the stability test, except for the significant drop (ca. 30%) in the propane conversion. The competitive adsorptions of CO₂ (or H₂O) and O₂, as well as C₃H₈, give rise to the decrease in catalytic performance. When 5 vol.% water vapor and 5 vol.% CO₂ are added into the reactant gas simultaneously, an interesting phenomenon occurs: the propane conversion value decreases by ca. 35%, which is the superposition of individual effects of water vapor and CO₂. Similarly, its original value is restored when the additional gas is cut off. These results indicate that CoCeO_x-70 maintains a stable structure after a long-time reaction under CO₂ and water vapor atmosphere. All these results reveal that CoCeO_x-70 can be efficiently used in simulated real conditions and that it exhibits good resistance to CO₂ and water vapor. Since stability is critical for the efficient use of a catalyst, the reusability of the catalyst also plays a significant role in the sustainability. It is observed that the T₅₀ and T₉₀ values of CoCeO_x-70 are maintained around 310 °C and 350 °C after be-

ing repeatedly tested 10 times under humid conditions, indicating that the CoCeO_x-70 catalyst exhibits favorable re-usability even in humid conditions.

3.4. *In situ* DRIFTS

In-situ DRIFTS is employed during propane adsorption and oxidation to obtain more detail of the reaction on the catalyst surface and to identify the evolved surface species. Figs. 11a and b show the *in-situ* DRIFTS spectra of the Co₃O₄ and CoCeO_x-70 catalyst in an atmosphere of C₃H₈/Ar (20 mL min⁻¹) at 50 °C. The strong adsorption peak at ~2964 cm⁻¹ with the shoulder peaks at 2871, 2902, and 2983 cm⁻¹ are assigned to the C–H vibration of propane gas [6,40,41]. The peaks between 1200 and 1600 cm⁻¹ are assigned to various carbonate species, such as polydentate CO₃²⁻ (~1340 cm⁻¹), δ_s (CH₃) (~1380 cm⁻¹), δ_{as} (CH₃) (~1470 cm⁻¹), and ν_{as} (COO⁻) (~1506 cm⁻¹) [40,42], the intensities of which increase with time of C₃H₈ exposure. A similar phenomenon is observed over the CoCeO_x-70 catalyst, indicating that Ce modification hardly changes the surface carbonate species during the propane adsorption. Afterward, the reactant gas is replaced by 0.2 vol.% C₃H₈, 5 vol.% O₂, and Ar balanced (20 mL min⁻¹), *in-situ* DRIFTS spectra over Co₃O₄ and CoCeO_x-70 are recorded after 20 min of reaction at 50–350 °C and shown in Figs. 11c and 11d. For pure Co₃O₄ (Fig. 11c), the

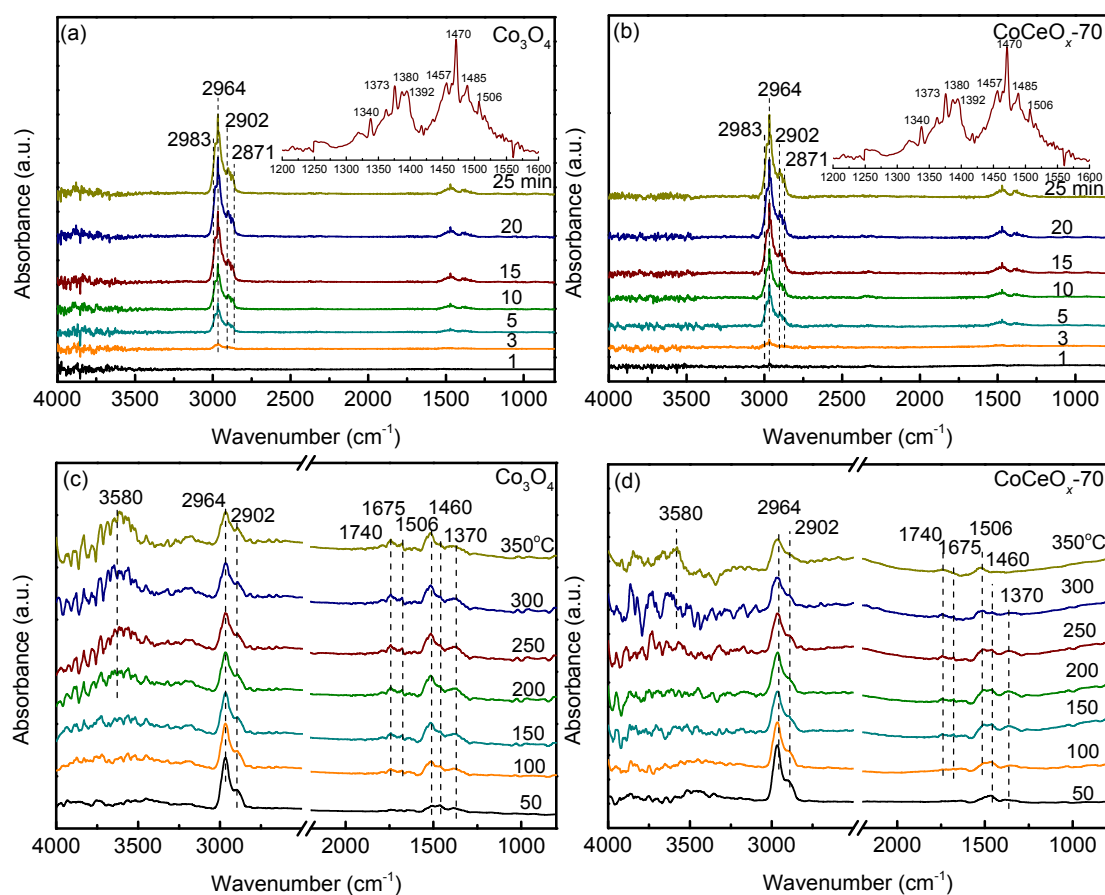


Fig. 11. *In-situ* DRIFTS spectra of the Co_3O_4 and $\text{CoCeO}_x\text{-70}$ catalyst: (a) and (b) under an atmosphere of $\text{C}_3\text{H}_8/\text{Ar}$ at 50°C ; (c) and (d) under an atmosphere of $0.2 \text{ vol.}\% \text{ C}_3\text{H}_8 + 5 \text{ vol.}\% \text{ O}_2/\text{Ar}$ at $50\text{--}350^\circ\text{C}$.

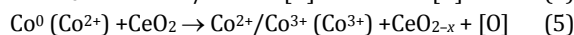
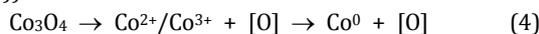
adsorption peaks of $\delta_s(\text{CH}_3)$ ($\sim 1370 \text{ cm}^{-1}$), $\nu_s(\text{COO}^-)$ ($\sim 1460 \text{ cm}^{-1}$), and $\nu_{\text{as}}(\text{COO}^-)$ ($\sim 1506 \text{ cm}^{-1}$) are observed at $< 100^\circ\text{C}$. With the further increase in the reaction temperature, new adsorption peaks appear at 1675 cm^{-1} and 1740 cm^{-1} , which are assigned to acetone $\nu(\text{C}=\text{O})$ and aliphatic ester species $\nu(\text{C}=\text{O})$, respectively [43–45]. Furthermore, the intensity of the adsorption peak assigned to the C–H vibration of propane ($\sim 2902 \text{ cm}^{-1}$ and $\sim 2964 \text{ cm}^{-1}$) decreases, and an adsorption peak assigned to hydroxyl species ($\sim 3580 \text{ cm}^{-1}$) emerges with continuously increasing temperature [46,47]. These illustrate that the species with C=O bonds participate in the propane total oxidation as intermediates. Similar peaks can be observed in the spectra recorded over the $\text{CoCeO}_x\text{-70}$ catalyst (Fig. 11d). However, the intensity of the adsorption peaks between 1200 and 1750 cm^{-1} noticeably decreases at $> 300^\circ\text{C}$, and the adsorption peaks indicative of $\delta_s(\text{CH}_3)$ (1370 cm^{-1}) and $\nu_s(\text{COO}^-)$ (1460 cm^{-1}) disappear at 350°C . This suggests that a highly effectively propane activation occurs on the $\text{CoCeO}_x\text{-70}$ surface. In other words, the presence of Ce in Co_3O_4 does not change the reaction mechanism of the propane total oxidation, but accelerates the C_3H_8 activation on the catalyst surface, leading to the improvement of the catalytic activity.

3.5. Discussion

The $\text{Co}_3\text{O}_4\text{-CeO}_2$ binary oxides exhibit superior activity to-

ward the catalytic oxidation of propane to those of single CeO_2 and Co_3O_4 catalysts, and the catalytic activity depends on the $\text{Co}/(\text{Ce}+\text{Co})$ molar ratios. Among $\text{Co}_3\text{O}_4\text{-CeO}_2$ binary oxide catalysts, $\text{CoCeO}_x\text{-70}$ exhibits the highest catalytic activity, and its T_{90} (GHSV = $120000 \text{ mL h}^{-1} \text{ g}^{-1}$) is 310°C . As shown in the TEM images, the particle size in the $\text{Co}_3\text{O}_4\text{-CeO}_2$ sample significantly decreases with the incorporation of Ce (agreeing with the XRD results), and the boundary between the nanoparticles obscures with uniform size distribution. These provide the possibility for the generation of the interaction between Co_3O_4 and CeO_2 , which would improve the low-temperature redox properties and thus enhance the activity [17]. The downshift of the reduction peaks in $\text{H}_2\text{-TPR}$ and $\text{C}_3\text{H}_8\text{-TPSR}$ profiles confirm that the Ce incorporation promotes the redox properties of the $\text{Co}_3\text{O}_4\text{-CeO}_2$ binary oxides. In the Raman spectra, the changes of the A_{1g} vibration indicate the distortion of the Co_3O_4 lattice, which can increase the oxygen vacancy concentration of the catalyst and provide lattice sites for oxygen migration. The $\text{O}_2\text{-TPD}$ and $\text{O}1s$ XPS analyses reveal that $\text{CoCeO}_x\text{-70}$ possesses abundant active oxygen species on the surface. It is widely recognized that high mobility of bulk oxygen (Mars-van Krevelen mechanism) and abundance of active oxygen species are the dominant factors influencing the catalytic activity of catalysts toward CH_4 , CO , and VOC catalytic oxidation [48–50]. According to the above results, an interaction between Co_3O_4 and CeO_2 is believed to occur, where the Co_3O_4 component can be partly

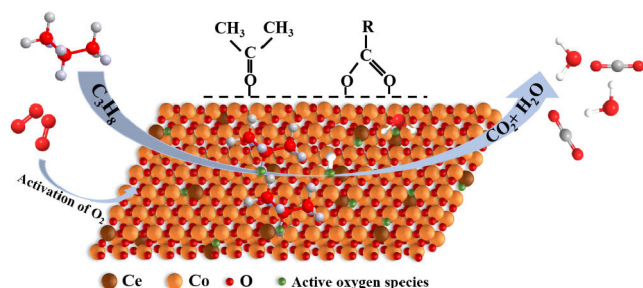
reduced to Co^{2+} or metallic Co by the reactant gas and oxygen vacancies are produced at the same time. Meanwhile, the reduced Co or Co^{2+} would combine with the oxygen species around the surrounding CeO_2 , generating a large number of oxygen vacancies nearby the Co_3O_4 – CeO_2 interface (Equations (4) and (5)).



These oxygen vacancies could react with oxygen and generate some active oxygen species, which could improve the catalytic activity. As shown in the *in-situ* DRIFTS spectra, the species with C=O bonds participate in the total oxidation of propane as intermediates, and the presence of Ce accelerates the activation of propane on the CoCeO_x -70 surface. Based on the *in-situ* DRIFTS analysis and various characterizations, a possible reaction pathway for the catalytic oxidation of propane over Co_3O_4 – CeO_2 binary oxide catalysts is proposed (as illustrated in Scheme 1). It is widely accepted that the total oxidation reaction of propane over transition metal oxides involves the Mars–van Krevelen mechanism, where propane is initially adsorbed on the surface of the lattice oxygen, of which the latter is re-oxidized by oxygen. After adsorption on the surface, propane is decomposed to produce carbonate species and subsequently oxidized to acetone and aliphatic ester species. Thereafter, the obtained ν (C=O) species undergo an oxidation process, which converts them into CO_2 and H_2O .

4. Conclusions

In this study, we demonstrate that an appropriate amount of Ce addition has a promotion effect on Co_3O_4 – CeO_2 catalysts toward the total oxidation of propane, and CoCeO_x -70 exhibits the highest activity ($T_{90} = 310$ °C, GHSV = 120000 mL h^{-1} g^{-1}). The enhancement in the catalytic activity of the CoCeO_x -70 catalyst toward the total oxidation of propane can be explained by the strong interaction between CeO_2 and Co_3O_4 , which results in an improvement of the low-temperature reducibility and generates additional oxygen vacancies and active oxygen species. *In-situ* DRIFTS analysis and reaction kinetics measurement confirm that Ce addition does not change the reaction mechanism of the propane catalytic oxidation, but accelerate the activation of propane on the surface. In addition, CoCeO_x -70 exhibits good resistance to CO_2 and water vapor during the long-term stability test, and no deactivation is observed after 10 usage cycles, providing the possibility for further industrial



Scheme 1. Mechanism of the propane catalytic oxidation over Co_3O_4 – CeO_2 binary oxides.

application.

References

- [1] M. N. Taylor, W. Zhou, T. Garcia, B. Solsona, A. F. Carley, C. J. Kiely, S. H. Taylor, *J. Catal.*, **2012**, 285, 103–114.
- [2] Y. Xie, Y. Yu, X. Gong, Y. Guo, Y. Guo, Y. Wang, G. Lu, *CrystEngComm*, **2015**, 17, 3005–3014.
- [3] Y. Boyjoo, H. Sun, J. Liu, V. K. Pareek, S. Wang, *Chem. Eng. J.*, **2017**, 310, 537–559.
- [4] Z. Zhu, G. Lu, Z. Zhang, Y. Guo, Y. Guo, Y. Wang, *ACS Catal.*, **2013**, 3, 1154–1164.
- [5] Z. Wang, Y. Liu, T. Yang, J. Deng, S. Xie, H. Dai, *Chin. J. Catal.*, **2017**, 38, 207–216.
- [6] Z. Hu, X. Liu, D. Meng, Y. Guo, Y. Guo, G. Lu, *ACS Catal.*, **2016**, 6, 2265–2279.
- [7] M. Cargnello, J. J. D. Jaén, J. C. H. Garrido, K. Bakhmutsky, T. Montini, J. J. C. Gámez, R. J. Gorte, P. Fornasiero, *Science*, **2012**, 337, 713–717.
- [8] J. E. Park, K. B. Kim, Y.-A. Kim, K. S. Song, E. D. Park, *Catal. Lett.*, **2013**, 143, 1132–1138.
- [9] Z. Hu, S. Qiu, Y. You, Y. Guo, Y. Guo, L. Wang, W. Zhan, G. Lu, *Appl. Catal. B*, **2018**, 225, 110–120.
- [10] C. Shi, Y. Wang, A. Zhu, B. Chen, C. Au, *Catal. Commun.*, **2012**, 28, 18–22.
- [11] D. Li, W. Li, Y. Deng, X. Wu, N. Han, Y. Chen, *J. Phys. Chem. C*, **2016**, 120, 10275–10282.
- [12] X. Xie, Y. Li, Z. Q. Liu, M. Haruta, W. Shen, *Nature*, **2009**, 458, 746–749.
- [13] C. Y. Ma, Z. Mu, J. J. Li, Y. G. Jin, J. Cheng, G. Q. Lu, Z. P. Hao, S. Z. Qiao, *J. Am. Chem. Soc.*, **2010**, 132, 2608–2613.
- [14] Z. Fan, Z. Zhang, W. Fang, X. Yao, G. Zou, W. Shangguan, *Chin. J. Catal.*, **2016**, 37, 947–954.
- [15] Z. Ren, Z. Wu, W. Song, W. Xiao, Y. Guo, J. Ding, S. L. Suib, P.-X. Gao, *Appl. Catal. B*, **2016**, 180, 150–160.
- [16] G. Salek, P. Alphonse, P. Dufour, S. Guillemet-Fritsch, C. Tenailleau, *Appl. Catal. B*, **2014**, 147, 1–7.
- [17] H. Li, G. Lu, D. Qiao, Y. Wang, Y. Guo, Y. Guo, *Catal. Lett.*, **2011**, 141, 452–458.
- [18] T. Montini, M. Melchionna, M. Monai, P. Fornasiero, *Chem. Rev.*, **2016**, 116, 5987–6041.
- [19] B. Zhao, Y. Jian, Z. Jiang, R. Albilali, C. He, *Chin. J. Catal.*, **2019**, 40, 543–552.
- [20] H. Wu, L. Wang, *Catal. Commun.*, **2011**, 12, 1374–1379.
- [21] L. Xue, C. Zhang, H. He, Y. Teraoka, *Appl. Catal. B*, **2007**, 75, 167–174.
- [22] C. Ma, D. Wang, W. Xue, B. Dou, H. Wang, Z. Hao, *Environ. Sci. Technol.*, **2011**, 45, 3628–3634.
- [23] T. Sato, T. Komanoya, *Catal. Commun.*, **2009**, 10, 1095–1098.
- [24] V. G. Hadjiev, M. N. Iliev, I. V. Vergilov, *J. Phys. C: Solid State Phys.*, **1988**, 21, L199–L201.
- [25] Q. Liu, L.-C. Wang, M. Chen, Y. Cao, H.-Y. He, K.-N. Fan, *J. Catal.*, **2009**, 263, 104–113.
- [26] I. Lopes, N. El Hassan, H. Guerba, G. Wallez, A. Davidson, *Chem. Mater.*, **2006**, 18, 5826–5828.
- [27] J. Luo, M. Meng, X. Li, X. Li, Y. Zha, T. Hu, Y. Xie, J. Zhang, *J. Catal.*, **2008**, 254, 310–324.
- [28] A. Martínez-Arias, M. Fernández-García, O. Gálvez, J. M. Coronado, J. A. Anderson, J. C. Conesa, J. Soria, G. Munuera, *J. Catal.*, **2000**, 195, 207–216.
- [29] Y. Luo, J. Zuo, X. Feng, Q. Qian, Y. Zheng, D. Lin, B. Huang, Q. Chen, *Chem. Eng. J.*, **2019**, 357, 395–403.

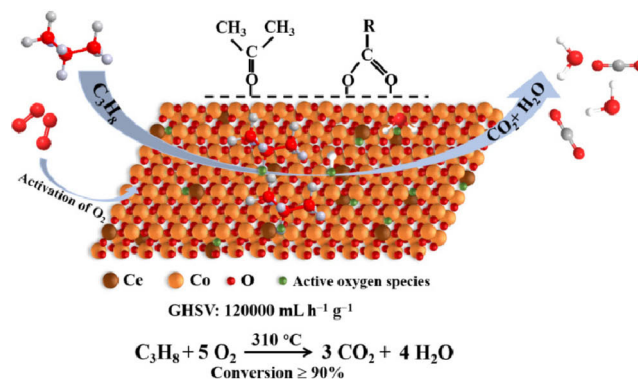
Graphical Abstract

Chin. J. Catal., 2020, 41: 679–690 doi: S1872-2067(19)63523-0

Insight into catalytic properties of Co₃O₄-CeO₂ binary oxides for propane total oxidation

Wenjun Zhu, Xiao Chen, Jianhui Jin, Xin Di, Changhai Liang*, Zhongmin Liu*
 Dalian University of Technology;
 Dalian National Laboratory for Clean Energy, Dalian Institute of Chemical Physics, Chinese Academy of Sciences

The strong interaction between Co₃O₄ and CeO₂ promotes the generation of oxygen vacancies and active oxygen species, which subsequently accelerate the activation of propane on the catalyst surface and promote the catalytic activity of Co₃O₄-CeO₂ catalysts toward the total oxidation of propane.



- [30] B. Bai, H. Arandiyani, J. Li, *Appl. Catal. B*, **2013**, 142–143, 677–683.
- [31] Y. Xia, H. Dai, H. Jiang, L. Zhang, *Catal. Commun.*, **2010**, 11, 1171–1175.
- [32] W. Ding, Y. Chen, X. Fu, *Catal. Lett.*, **1994**, 23, 69–78.
- [33] Y. Liu, H. Dai, J. Deng, Y. Du, X. Li, Z. Zhao, Y. Wang, B. Gao, H. Yang, G. Guo, *Appl. Catal. B*, **2013**, 140–141, 493–505.
- [34] W. Tang, X. Wu, S. Li, X. Shan, G. Liu, Y. Chen, *Appl. Catal. B*, **2015**, 162, 110–121.
- [35] A. Restovic, E. Ríos, S. Barbato, J. Ortiz, J. L. Gautier, *J. Electroanal. Chem.*, **2002**, 522, 141–151.
- [36] A. Bielanski, J. Haber, *Oxygen in Catalysis*, Marcel Dekker, New York, **1991**.
- [37] Y. Moro-Oka, Y. Morikawa, A. Ozaki, *J. Catal.*, **1967**, 7, 23–32.
- [38] J. Wu, Q. Xia, H. Wang, Z. Li, *Appl. Catal. B*, **2014**, 156–157, 265–272.
- [39] H. Pan, M. Xu, Z. Li, S. Huang, C. He, *Chemosphere*, **2009**, 76, 721–726.
- [40] Z. Hu, Z. Wang, Y. Guo, L. Wang, Y. Guo, J. Zhang, W. Zhan, *Environ. Sci. Technol.*, **2018**, 52, 9531–9541.
- [41] Y. Xie, Y. Guo, Y. Guo, L. Wang, W. Zhan, Y. Wang, X. Q. Gong, G. Lu, *Catal. Sci. Technol.*, **2016**, 6, 8222–8233.
- [42] S. Swislocki, K. Stöwe, W. F. Maier, *J. Catal.*, **2014**, 316, 219–230.
- [43] C. P. O'Brien, I. C. Lee, *J. Catal.*, **2017**, 347, 1–8.
- [44] M. Baldi, E. Finocchio, F. Milella, G. Busca, *Appl. Catal. B*, **1998**, 16, 43–51.
- [45] L. Ma, C. Y. Seo, X. Chen, K. Sun, J. W. Schwank, *Appl. Catal. B*, **2018**, 222, 44–58.
- [46] X. Wu, L. Zhang, D. Weng, S. Liu, Z. Si, J. Fan, *J. Hazard. Mater.*, **2012**, 225–226, 146–154.
- [47] F. Liu, J. Shen, D. Xu, W. Zhou, S. Zhang, L. Wan, *Chem. Eng. J.*, **2018**, 334, 2283–2292.
- [48] M. Luo, Y. Cheng, X. Peng, W. Pan, *Chem. Eng. J.*, **2019**, 369, 758–765.
- [49] P. Xu, Z. Wu, J. Deng, Y. Liu, S. Xie, G. Guo, H. Dai, *Chin. J. Catal.*, **2017**, 38, 92–105.
- [50] D. Widmann, R. J. Behm, *J. Catal.*, **2018**, 357, 263–273.

Co₃O₄-CeO₂氧化物对丙烷完全氧化的催化性能

朱文军^{a,b}, 陈霄^a, 金建辉^a, 邸鑫^a, 梁长海^{a,*}, 刘中民^{b,#}

^a大连理工大学精细化工国家重点实验室, 先进材料与催化工程实验室, 辽宁大连116024

^b中国科学院大连化学物理研究所, 中国科学院洁净能源创新研究院, 甲醇制烯烃国家工程实验室, 辽宁大连116023

摘要: 挥发性有机化合物(VOCs)是全球大气污染物的主要来源, 近年来已造成严重的环境问题. 催化氧化是一种有效的、经济可行的VOCs去除技术, 其研究的关键在于开发高效、稳定的催化剂. 在本文中, 我们采用柠檬酸法合成了一系列具有不同Co/(Ce+Co)摩尔比的Co₃O₄-CeO₂二元氧化物催化剂, 研究了其对丙烷(低碳VOCs)的催化氧化性能.

在催化活性测试中, 反应气的组成为0.2 vol.% C₃H₈和5 vol.% O₂, Ar为平衡气, 气体总流速为200 mL min⁻¹. 实验结果表明, Ce的掺入能够明显提高Co₃O₄的丙烷催化氧化性能, Co₃O₄-CeO₂催化剂的丙烷催化氧化活性顺序为CoCeO_x-70 > CoCeO_x-90 > Co₃O₄ > CoCeO_x-50 > CoCeO_x-20 > CeO₂. 当Co/(Ce+Co)摩尔比为70%时, CoCeO_x-70催化剂的丙烷催化氧化性能最好. 在丙烷转化率达到90%时, CoCeO_x-70催化剂的反应温度为310 °C (GHSV = 120000 mL h⁻¹ g⁻¹), 相比于单一的Co₃O₄催化剂的反应温度降低了25 °C.

XRD和TEM表征结果显示, 在Co₃O₄-CeO₂二元氧化物催化剂中存在Co₃O₄和CeO₂两种晶型, 同时随着Ce的掺入, 催化剂的粒径明显降低. Raman光谱图显示, Ce的掺入使催化剂的晶格发生畸变, 促进催化剂表面氧空位的产生, 为催化剂中氧的迁移提供晶格位点. H₂-TPR和C₃H₈-TPSR结果表明, Co₃O₄与CeO₂间存在相互作用, 能够提高催化剂的低温还原性能, 以促进催化剂的丙烷催化氧化. O₂-TPD和O 1s XPS结果表明, Ce的掺入能够增加催化剂表面活性物种的产生, 提高催化剂

中氧的移动性,从而提高了催化剂对丙烷的催化氧化活性.在对 Co_3O_4 和 CoCeO_x -70催化剂进行 $in-situ$ DRIFTS表征和简单的动力学研究,我们发现Ce的掺入不改变催化剂的丙烷催化氧化反应路径,其存在能够促进丙烷在催化剂表面的吸附和活化,以提高催化剂的丙烷催化氧化活性.同时,丙酮和酯作为中间物参与到丙烷的催化氧化反应过程中.

此外,我们考察了反应气氛中水蒸气和 CO_2 的存在对催化剂催化性能的影响.结果表明, CO_2 和水蒸气的存在都抑制了催化剂的丙烷催化氧化活性,催化性能随着 CO_2 和水蒸气浓度的增加而降低.在相同条件下,水蒸气对催化剂催化性能的抑制作用明显大于 CO_2 的抑制作用,但这种抑制作用会随着反应气中水蒸气和 CO_2 的消失而消失.在稳定性测试中, CoCeO_x -70催化剂表现出优异的抗水蒸气和 CO_2 性能.在反应气中存在5 vol.%水蒸气和5 vol.% CO_2 的条件下, CoCeO_x -70催化剂在50 h的稳定性测试中均未出现明显的失活现象.同时,经过10次加热和降温循环测试后,催化剂的催化活性也没有发生明显变化,这为 CoCeO_x -70催化剂的未来工业化的应用提供了可能.

关键词: 丙烷; 完全氧化; Co_3O_4 - CeO_2 ; 原位漫反射傅里叶变换红外光谱; 挥发性有机化合物

收稿日期: 2019-08-22. 接受日期: 2019-09-30. 出版日期: 2020-04-05.

*通讯联系人. 电话: (0411)84986353; 电子信箱: changhai@dlut.edu.cn

#通讯联系人. 电话: (0411)84379998; 电子信箱: liuzm@dicp.ac.cn

基金来源: 国家重点研发计划(2016YFB0600305).

本文的电子版全文由Elsevier出版社在ScienceDirect上出版(<http://www.sciencedirect.com/science/journal/18722067>).